MetaSoil: Passive mmWave Metamaterial Sensor for Multi-layer Soil Moisture Sensing

Baicheng Chen
University of California San Diego
La Jolla, CA, USA
b3chen@ucsd.edu

John Nolan
University of California San Diego
La Jolla, CA, USA
jmnolan@ucsd.edu

Xinyu Zhang
University of California San Diego
La Jolla, CA, USA
xyzhang@ucsd.edu

Wan Du
University of California Merced
Merced, CA, USA
wdu3@ucmerced.edu

Abstract

Soil moisture level sensing is essential for enabling smart irrigation, which is crucial for our food security and sustainable agriculture. Existing soil moisture sensing systems face limitations such as single-layer sensing, limited depth, power supply reliance, and complex calibration. In addition, costly and cumbersome sensor unit design hinders mass and dense deployment of passive intelligence. This paper introduces MetaSoil, a soil moisture sensing system that is calibration-free, continuous, and multi-layered, leveraging a passive 3D printable mmWave metamaterial. When soil moisture level changes, our hydrogel patched polylactic acid (PLA) metamaterial alters resonant frequency in the impinging mmWave signals due to impedance match offset. Our system eliminates in-soil power supply dependencies by utilizing the RF resonance of 3D-printed metamaterial, allowing for deeper placement, and simultaneous multi-layer sensing. We then integrate a commercial-off-the-shelf (COTS) mmWave radar to query the metamaterial sensor. With MetaSoil's fully passive metamaterial pole, RF signal from far is redirected towards the sensor unit, bypassing soil's heavy attenuation effect. Through our extensive evaluation, MetaSoil achieves 98.9 % accuracy with ±10% moisture level precision in single-layered sensing, at depth of 1m meter. It achieves 98.8 % accuracy with ±10% in double layered sensing at same depth with 10cm sensor spacing. We further examine the robustness of our system with real-world requirements. Overall, MetaSoil represents a low-cost, durable, and easily deployable solution that supports remote and continuous soil moisture monitoring, advancing the scalability and effectiveness of smart agricultural practices.

CCS Concepts

• **Computer systems organization** → **Embedded and cyber-physical systems**; • **Networks** → **Mobile networks**.

Keywords

mmWave Sensing, Metamaterial, Smart Agriculture, IoT

ACM Reference Format:
Baicheng Chen, John Nolan, Xinyu Zhang, and Wan Du. 2024. MetaSoil: Passive mmWave Metamaterial Sensor for Multi-layer Soil Moisture Sensing . In *ACM Conference on Embedded Networked Sensor Systems (SenSys '24), November 4–7, 2024, Hangzhou, China.* ACM, New York, NY, USA, 14 pages. https://doi.org/10.1145/3666025.3699334

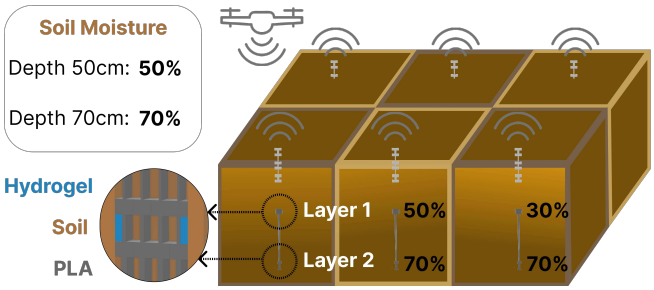

Figure 1: MetaSoil is a passive mmWave metamaterial sensor aided multi-layer soil moisture level sensing system. With accessible material and fabrication techniques, MetaSoil can replace existing smart agriculture soil moisture monitoring systems with low cost and denser sensor deployment.

1 Introduction

Smart agriculture directly supports food security [5, 23, 38, 59]. By continuously monitoring soil moisture levels, farmers can avoid overwatering or underwatering [14, 40], which harms crop production. In addition, smart irrigation systems help conserve water resources, reduce labor costs, and promote sustainable farming practices. Thus, it is important to develop an efficient and effective soil moisture sensing mechanism to enable large-scale smart irrigation.

Traditionally, soil moisture level is sensed with direct current (DC) capacitance sensors that measure the DC dielectric permittivity of the soil surrounding the sensor [43]. In recent years, wireless approaches have been explored that remove cables and attempt to deploy at a large scale. However, existing systems have their own limitations. First, [34] proposed a sensor-free configuration

SenSys '24, November 4–7, 2024, Hangzhou, China

ACM ISBN 979-8-4007-0697-4/24/11
https://doi.org/10.1145/3666025.3699334

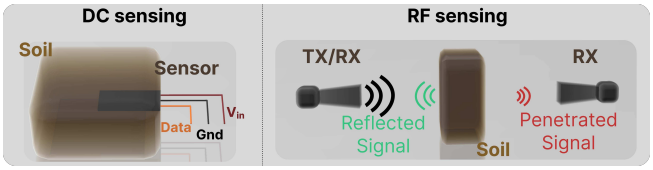

Figure 2: Traditional soil moisture sensing mechanisms have obvious deployment limitations. Wired sensors require constant power supply, while its metal probe can corrode over time. Wireless sensors relying on radio frequency signal propagation pattern are limited to shallow soil down to ≈40cm and losses signal completely at high soil moisture.

that offers an algorithmic approach to multilayered moisture level detection, yet its applicability is limited to the soil surface due to its physical attenuation constrains. Similarly, [56] relies on RFID tags in/on pots that are agile but suffer the same limitation of attenuation when placed underneath a field. Next, [15, 19, 25, 48, 57] buries sensors/receivers under the soil and measures different ratios of attenuation. Such a technique requires digging for both placement and maintenance, and the need of power supplies makes it unpractical for large scale deployments. Lastly, [31] presents a passive metal circuit design that can be buried under the soil with a Wi-Fi antenna extends over the soil surface, but a metal plate is completely in contact with the soil, which can easily be corrupted and contaminated. Overall, all of the above sensing mechanisms require a calibration scheme for different soil compositions, which is obfuscating the real-world usage. In addition, most systems fail to support crop diversity such as deep-root crops (e.g., grape, olive, and almond), which requires depth to be extended to 15 ft [55]. Although each of the work presents their solution to partially solve the problem, their limitations still hinder the large scale smart agriculture application.

To this end, we present MetaSoil, a **i) fully passive**, **ii) calibration free**, **iii) continuous**, and **iv) multi-layered** soil moisture sensing system based on the 3D printable mmWave metamaterial. The overall sensing scheme is presented in Fig. 1. To maximize scalability in large scale smart agriculture applications, we completely remove the power supply constraint by utilizing RF resonance of 3D printed polylactic acid (PLA) metamaterial sensor to direct the signal downward. With a low-cost and durable metamaterial sensor [44], we also unlock sensing with multi-layer depths simultaneously and push the depth to 1.5m and deeper. We then remove the calibration process to fit one sensor with any soil moisture level sensing application by using a low-cost commercial-off-the-shelf (COTS) hydrogel patch as a moisture holding mediator. A Frequency Modulated Continuous Wave (FMCW) mmWave radar is then placed on top to remotely and continuously interrogate the resonance responses from the metamaterial sensor. This can be done either manually or through automated machines (e.g., a drone or mobile robot).

To attain the desired functionalities, MetaSoil is designed to overcome the following key challenges:

i) Fully passive sensor: soil naturally attenuates the mmWave signal severely with its moisture content. Such attenuation can be ambiguous in contrast to background noise and path loss in the field. To clearly identify soil moisture level with a passive sensor, we propose a 3D printed metamaterial sensor design that matches impedance with the soil and reflects impedance match offset when soil moisture level changes.

ii) Multivariate soil composition: soil is also highly diverse in composition. Two samples in the same orchard can have a very different composition due to topographic variation, rain, and fertilization [42]. This also leads to different impedance characteristics in the radio frequency (RF) domain, which would require traditional sensing systems to perform per-site calibration. To eliminate the need, we present a hydrogel-mediated approach to interface with soil moisture. Hydrogels are durable polymers that are capable of repeating the storage and donating of water based on the moisture level of the soil in contact [16]. We first verify the hydrogel's wetting and drying moisture level curve compared to that of the soil; then, we employ adhesive hydrogel to the part of the metamaterial sensor where resonance is optimized. As the hydrogel water content changes, its shape and dielectric value change, causing a significant resonant frequency shift.

iii) Multi-layer signal attenuation: soil has a much higher dielectric loss compared to air and PLA material, with multilayer sensing, the loss will increase exponentially per millimeter of soil. Instead of having multiple soil layers, we utilize the metamaterial sensor to resonate at different layers with the soil in contact. Each layer of the metamaterial can be designed as a sensor layer that exchanges a small portion of its PLA structure for soil. As the soil moisture level changes, the resonance of that specific layer will also change. This allows multiple layers of soil to be sensed simultaneously without having to worry top layer of soil attenuating the bottom layer signal.

iv) Radar signal path optimization: ideally, the radar is perfectly perpendicular to the ground, so that the antenna points directly down to the metamaterial pole. While we want to maximize the amount of signal from the radar that is passed down the pole structure, the radar may be moving on the land and have varying sensing angles. To improve the robustness of the system against the radar position variation, we design arrays of metaatoms that process ±45° incident waves, with the exit wave directed straight down the pole. This also has the side benefit of spatial encoding from the radar received signal such that every interval of incident angle will generate a unique downstream signal signature. This enables accurate modeling of the signal model from air all the way down to the last soil layer being sensed.

We prototype a metasurface sensor in the form of a 10x10x100 cm (LxWxH) long pole using 3D printable PLA material at a total cost of less than US$20. We conduct experiments in real-world setup where the metasurface sensor is buried in soil with only Director protruding. Throughout extensive evaluation, MetaSoil has proven its accuracy with accuracy of 98.9% in single-layer moisture level sensing tasks and accuracy of 98.8% in double-layer moisture level sensing, with ±10% precision tolerance. From 0 to 100 % soil moisture level dynamic range, MetaSoil's prediction achieves a nearly perfect correlation of $R^2 = 0.98$. In addition, MetaSoil's performance maintained above 98% when stress was tested on the sensor depth up to 1m, the distance between the radar and the pole up to 1.5m, and the angle of inclination of the radar and the pole of ±50°. Furthermore, MetaSoil works robustly with 3 different types of soil compositions.

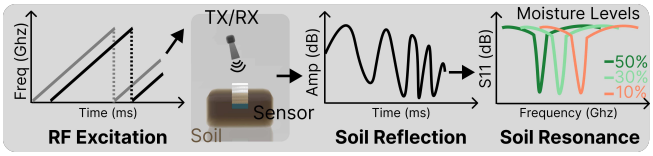

Figure 3: MetaSoil leverages a dielectric resonator and RF query device to extract soil moisture level under soil surface. As the hydrogel patch under dielectric resonator changes its water content along with soil moisture level, the whole sensor's resonance varies accordingly.

To this end, we conclude the following contributions:

- We design and fabricate a completely passive, wireless soil moisture sensing platform using 3D printable dielectric mmWave metamaterial sensor.
- We unlock calibration-free multilayer sensing on a single metamaterial sensor.
- We optimize the metamaterial sensor to accept a wide range of sensing signals from above the ground.
- We develop corresponding signal processing and regression model for accurate multi-layered soil moisture level detection.
- We perform extensive evaluations on the accuracy and robustness of the soil moisture sensing system in real-world scenarios.

2 Preliminaries

2.1 Soil Dielectric Resonance

Soil composition can be divided into two categories, organic and inorganic materials [51]. Inorganic material (e.g., sand, silt, clay, > 90%) of different sizes make up the structure of the soil with water adhesion, while organic material (e.g., plant, animal remains, < 10%) [22]. These materials can be modeled as a dielectric layer with a moisture level directly proportional to their DC dielectric permittivity [58]. When broadband RF waves illuminate a layer of soil, portions of the wave are reflected and scattered, while the remainder penetrate the soil with moisture level-dependent attenuation, as demonstrated in previous works [25, 34, 56]. In addition, deep soil can be sensed with the dielectric resonance method, demonstrated by a DC circuit system [31]. Although soil does not naturally have an observable high-frequency resonant point, a resonating structure that brings soil into contact as a layer in its whole structure can give us the intrinsic property of the soil, such as permittivity correlated moisture level.

Hypothesis: Different amounts of water within the same soil space will change the dielectric permittivity of the soil layer, which in turn alters the amount of energy being reflected, scattered, and passed through. Different 3D geometry of the resonating structure can be designed and optimized to focus on a specific layer of material, which, in turn, maximizes the effect of dielectric permittivity change on the response signal. Thus, we hypothesize that *employing a passive dielectric resonating structure that assimilates a layer of soil will allow observation of varying soil moisture levels when illuminated by wireless signals.*

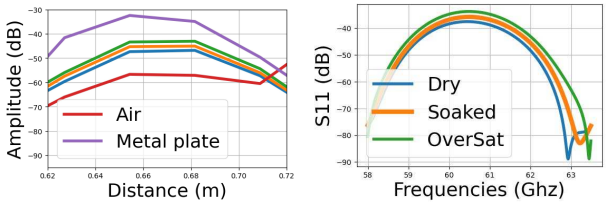

(a) Radar reflection compared to air or metal sheet.

(b) Soil resonant frequency with varied moisture levels.

Figure 4: Evaluation result clearly indicates strong correlation between soil moisture level and its capability to be sensed remotely with a metamaterial sensor. Dry soil is oven dried for 2 hours, soaked soil is dry soil at 100% moisture level, and oversat soil is adding more water to soaked soil sample.

2.2 RF Dielectric Resonance Modeling

In the past, dielectric material in grating pattern have been explored to form bianisotropic metamaterial for impedance matching and resonance effect [46]. Fundamentally, RF propagation follows Snell's law[9], when RF wave arrives a boundary between two materials with different dielectric permittivity, reflection and refraction of wave occur based on the ratio of permittivity difference. Leveraging recent advances in COTS 3D printing systems with micrometers of precision, we design a metamaterial that bridges RF impedance for air and soil. An n-layered grating shows the following wave propagation characteristics:

$$\mathbf{M}^{sensor} = \mathbf{M}^{1}_{\text{interface}}\mathbf{M}_{\text{delay}}\mathbf{M}^{2}_{\text{interface}}\cdots\mathbf{M}_{\text{delay}}\mathbf{M}^{n}_{\text{interface}} \tag{1}$$

where $\mathbf{M}^{sensor}$ is the whole dielectric structure's wave network matrix, $M^{1}_{interface}$ represents the geometric wave propagation behavior for layer 1, and M_{delay} represents the time delay pattern. As the RF signal propagates through the structure, each layer's wave network matrix is multiplied by the next layer's wave network matrix. Each wave network matrix $\mathbf{M}$ is a 2x2 matrix that represents the reflection and transmission of the RF signal at the boundary of the dielectric material.

$$\begin{aligned}\mathbf{M}_{\text{interface}} &= t_x \otimes \begin{pmatrix}1 & 0\\ 0 & 0\end{pmatrix} + t_y \otimes \begin{pmatrix}0 & 0\\ 0 & 1\end{pmatrix},\\ \mathbf{M}_{\text{delay}} &= \Phi_x \otimes \begin{pmatrix}1 & 0\\ 0 & 0\end{pmatrix} + \Phi_y \otimes \begin{pmatrix}0 & 0\\ 0 & 1\end{pmatrix}\end{aligned} \tag{2}$$

$\otimes$ is the Kronecker tensor product, T_u and R_u are the Fresnel transmission and reflection coefficients:

$$\mathbf{t}_u = \frac{1}{T_u}\begin{pmatrix}1 & R_u\\ R_u & 1\end{pmatrix}, \quad \Phi_u = \begin{pmatrix}e^{i\varphi_u} & 0\\ 0 & e^{-i\varphi_u}\end{pmatrix} \tag{3}$$

u can be substituted with either x or y referring to x or y axis polarization, respectively. t and Φ are the amplitude and phase modulations that a layer applies to incoming RF signal.

$$R_u = \frac{\eta_u - \eta_0}{\eta_u + \eta_0}, \quad T_u = \frac{2\eta_u}{\eta_u + \eta_0} \tag{4}$$

$$\eta_u = \frac{\eta_0}{\sqrt{\epsilon_{ru}(\omega)}}, \quad \varphi_u = \varphi_0\sqrt{\epsilon_{ru}(\omega)}, \quad \varphi_0 = k_0 d \tag{5}$$

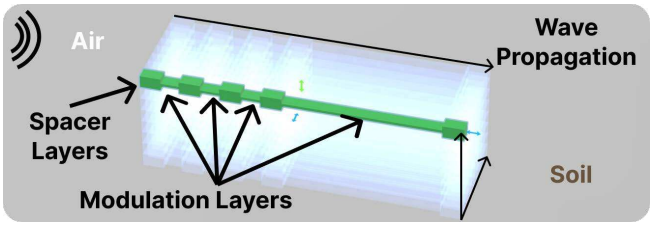

Figure 5: MetaSoil dielectric resonator structure for proof of concept experiment. The translucent parts are replicas of the structure in the axis perpendicular to wave propagation.

and η_0 is free space wave impedance, $\epsilon_{ru}(\omega)$ is the frequency dependent relative effective permittivity for a given layer. φ_0 is the electrical thickness of the layer in terms of wavelength, d is the physical thickness, k_0 is the propagation constant in free space.

$$\epsilon(\omega) = \sum_{m}^{M} p\epsilon_m(\omega) \tag{6}$$

where $\epsilon(\omega)$ is the frequency dependent dielectric constant for a layer of dielectric material, given p% of material m. M is the set of all materials in a given layer. In our application, the n-th layer is the soil layer, where as the 1st to $(n-1)$-th utilizes proportions of dielectric material and air to achieve various refraction goals.

2.3 Proof of Concept Study

Following the above principle, we first fabricate a dielectric resonator design that matches the impedance from air to soil, which has an ϵ value of 1 and 5, respectively. We utilize 60 GHz high-frequency RF signal with short wavelength of 5mm. The basic resonator design has 4 modulation layers and 5 spacer layers that hold the structure with a total thickness of 2cm. Fig. 5 and Fig. 4(a) illustrate the 3D geometry of the structure and the work flow, respectively. The result is shown in Fig. 4(a) and Fig. 4(b). A different moisture level of soil layer is reflected in radars' return signal, and further interpolated resonant frequency offset. Under radar sight, measurements from free space (i.e., substituted with air) and a strong reflector (e.g., aluminum plate) serve the minimum and maximum reflection strength for calibration. To this end, we conclude that a passive dielectric resonant structure can be used to sense the soil moisture level of specific layers.

2.4 Hydrogel Mediator

Soil at its dry form with different composition of organic and inorganic material can have various radio frequency dielectric constants ranging from $3-6$ [30, 50]. As shown in Fig. 6, different compositions with different grain of particles lead to different sizes of air holes, which make up different water retention capacities. With higher moisture level, the average dielectric constant value of the same soil block is pulled towards ~ 13, which is the dielectric constant of water at the same frequency [39]. To mitigate the need to calibrate for minimum and maximum dielectric constants, our MetaSoil system opts for a material-mediated sensing approach using a water-retaining hydrogel [32]. Given the ability of the hydrogel to retain water at a higher rate than soil, it has been used

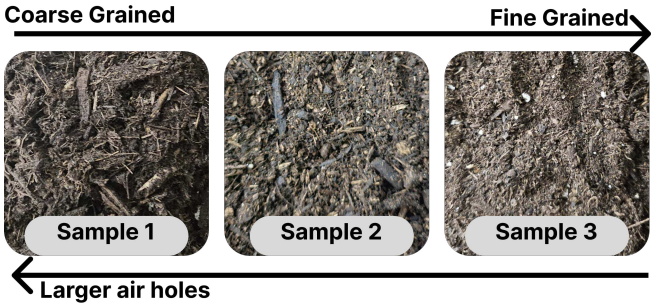

Figure 6: Different soil compositions with different physical texture. Coarser grained soil with larger material such as tree bark, plant stem, and gravel/pebbles lead to larger air holes that allow water to pass through easily, which leads to poorer water retaining capability.

to cure droughts by mixing it with soil [1, 26, 53]. Its water absorbing and donating characteristic is similar to that of the soil, which allows the plant roots to directly obtain water at a consistent rate over a longer period of time [32]. As shown in Fig. 7, the moisture level of the hydrogel and soil is synchronized quickly after drastic changes in the moisture level such as irrigation. It is also worth mentioning that the hydrogel inherits the durability and safety of the polymer material from both plants and humans [2, 16]. To this end, we have a high-level construction of a completely passive soil moisture level sensing system using an RF resonant dielectric sensor with hydrogel mediator.

3 System Overview

MetaSoil is a fully passive mmWave metamaterial sensor-assisted soil moisture sensing system that uses hydrogel as a mediator. An end-to-end system overview is shown in Fig. 8.

3.1 MetaSoil Sensor Infrastructure

MetaSoil's primary physical infrastructure is the passive mmWave metamaterial sensor that resonates with soil in its surrounding. The passive metamaterial sensor uses ubiquitous and accessible material such as PLA that allows rapid prototyping and deployment. The

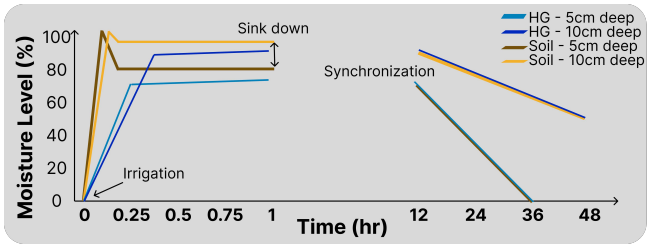

Figure 7: Soil and hydrogel have different water adoption and releasing rates, however, in short period of time (i.e., 1 hour), the two material's moisture level synchronizes themselves. To compensate the difference, MetaSoil interpolates hydrogel moisture level to soil moisture level.

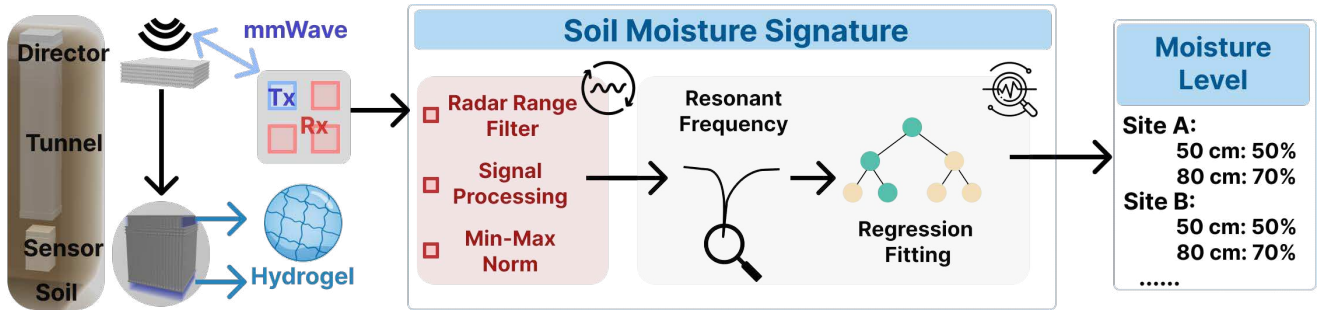

Figure 8: MetaSoil remotely queries pole at different depth, performs signal processing, extract soil resonance signature, and identifies moisture level. mmWave signal passes through the Director, Tunnel, and Sensor to reach targeted soil layer. The Sensor's geometric design then resonates with attached hydrogel material, and reflects remaining signal back to the radar receiver. The received signal then go through a series of signal processing steps to extract soil moisture level at different depths.

metamaterial sensor is a *pole*-shaped structure that extends from above the ground to as far as needed under the soil while occupying only a small volume relative to the farm. The pole consists of a **Director** above the ground that manages wave propagation, a **Tunnel** that maximizes signal reaching depth, and the **Sensor** that resonates with deep soil and responds to the signal embedded with moisture level. Each component is easy to print and assemble, highly customizable, and resistant to corrosion.

3.2 MetaSoil Sensing Strategy

MetaSoil utilizes COTS mmWave radar that remotely interrogates and processes the metamaterial pole's resonance with different layers of soil. The radar transmits the FMCW signal with large bandwidth and captures the reflected signal from the pole for soil signature decoding. Once the signal is received, the signal extraction module first performs range bin filtering and noise cancellation, which searches for the soil resonance signature. Signal processing techniques are then applied in the time and frequency domains to extract the resonance pattern. Lastly, a regression-based algorithm takes the resonance signal pattern as input and outputs each layer's moisture level.

4 Sensor Design

In this section, we first explicitly describe design principles and optimization goals towards the Director, Tunnel, and Sensor components on the pole-shaped metamaterial. Then, we detail the remote mmWave radar's signal modulation, processing algorithms, and machine learning model for an end-to-end soil moisture level sensing workflow.

4.1 MetaSoil Pole

4.1.1 Pole-Director and Sensor. The Director and the Sensor are two separable pieces of the dielectric metamaterial pole, each comprising multiple sensing layers of dielectric grating held together by spacer layers. The Director guides signal from centimeters protruded above soil surface straight down into the Tunnel, and the Sensor are buried deep under soil to interact with soil. They are uniformly designed to guide signal with top layer protruding soil surface, and bottom layer maximizing resonance on soil sensing layers. Fixed size spacers are used to hold different layers together as layers with different ratios of PLA and air-infill redirect RF signal.

Its worthy to note that soil with different grain size in its composition leads to different size of air holes. Larger air holes not only have higher permittivity for water to flow through, they also allow more RF energy to pass through, leading to lower reflection strength. To remove the sensor's need to calibrate for each type of soil, we apply hydrogel patches that are low cost and durable to interact with soil moisture.

A 3D printed illustration of the whole structure is shown in Fig. 9(a). Generally, with increasing complexity in the number of layers, the structure will provide more degrees of freedom for frequency selectivity, which leads to finer-grained control in frequency-limited scenarios. However, after 5 layers of design, the resonant amplitude is maximized (i.e., the reflection amplitude is minimized) and further optimization would lead to overfit, as shown in Fig. 9(b). We thus allocate 5 layers to the Director and 5 layers to the Sensor. The Tunnel with variable length and no PLA infill is also modeled as a

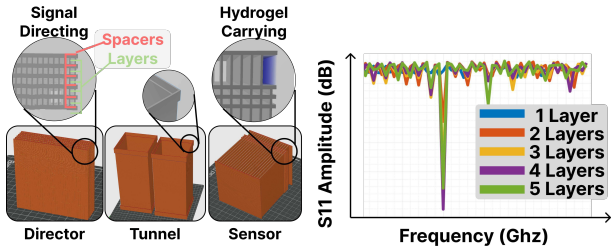

(a) MetaSoil 3D view on Director, Tunnel, and Sensor design.

(b) Marginal resonance amplitude upon 5 layers of complexity.

Figure 9: Director/Tunnel/Sensor are fully passive, 3D printable components that enables deep soil sensing. The Director and Sensor both comprise multiple sets of Spacer-Layer patterns for impedance matching and resonance purposes. The Tunnel has a modular design that extends or shrinks the pole while maintaining impedance matching. Without any of the three components, the resonance will not be as effective as shown in (b).

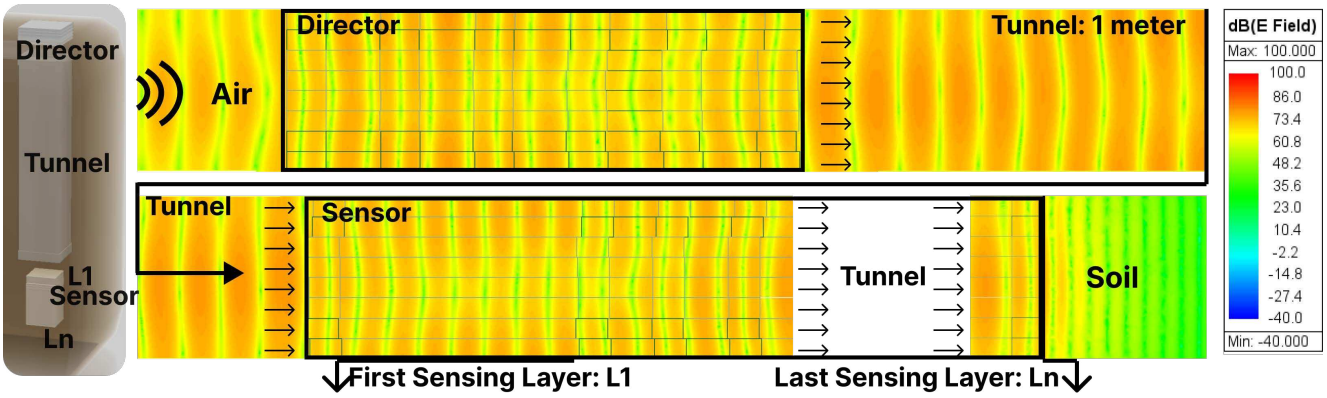

Figure 10: HFSS electric field plot heat map that shows strong signal level across air, Director, Tunnel, Sensor, and soil layers. The simulation extends soil layer until signal completely attenuates which is generally true in farms. In between Layer 1 (L1) and Layer n (Ln), user can repeat sensing layers to achieve multi-layered sensing. In addition, the modular Tunnel structure allows user to extend or shrink the pole while maintaining impedance match.

thick layer of air interconnecting the Director and the Sensor. Such design enables the impedance matching capability of the entire structure without compromising signal loss along the narrow and long metamaterial pole.

4.1.2 Pole-Tunnel. Ideally, the pole's Tunnel is an integral design that directly links the Director and the Sensor with PLA material. However, PLA material itself has a dielectric permittivity of around 2.96 and a dielectric loss of around 0.02 [24], which still causes the mmWave signal to be lossy than air. In simulation, a layer of 2% PLA infill with 460 mm thickness would lead to $\sim 25dB$ propagation loss. while a layer of 0% PLA infill (i.e., pure air) would allow the signal to travel further without significant loss in our application. While varying the thickness of the tunnel layer, we can optimize the whole structure to maintain the impedance matched. In addition, repeated patterns of fine-grained structure in bulk significantly increase the print time. However, removing the structure introduces a less controlled signal propagation pattern inside the Tunnel, which sacrifices SNR. In MetaSoil, we take the trade-off that maximizes the signal propagation path distance and leave the inside of the Tunnel completely free of PLA material.

4.2 Different Incident Angles

The above Director optimizes for maximizing propagation depth for 0 degree incidental wave, real world sensing deployment might require more usability with various probing angles. Instead of repeating the metaatom across the 2D surface, we design an array metaatoms that turn incidental wave at angles from 0 to 35 degrees to 0 degree existing the bottom of Director. The metaatom array is demonstrated in Fig. 11, and the signal propagation strength is also shown in Fig. 12. A complete view on signal strength while propagating from Director to Sensor is shown in Fig. 10.

4.3 Multi-layer optimization

We further design the MetaSoil structure to enable simultaneous multi-layer soil moisture level sensing. At target distances, a large window (e.g., 1cm) is opened to place the hydrogel on the side; the window size can be customized to fit different types of hydrogel available (e.g., patch, prism, beads). As shown in Fig. 13, the hydrogel is placed on the bottom layer of the Sensor for a simple single layer setup, bottom and side for two or more layers. With 60Ghz mmWave radar's 5.5GHz bandwidth, the range resolution is 2.7cm,

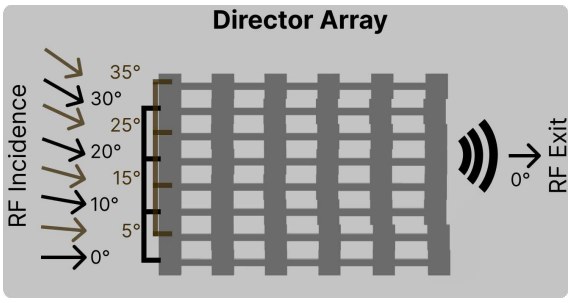

Figure 11: MetaSoil Director metaatom array unites multiple discretely optimized metaatoms to collectively form a metamaterial that redirects RF wave propagation direction.

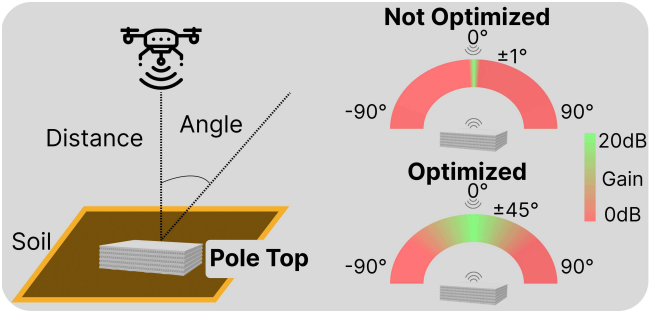

Figure 12: Leveraging metaatoms optimized for various incident angles, MetaSoil's fully passive Director array gains 20dB signal strength across ±45° RF incident angle.

which gives us fine-grained spatial resolution down the pole. As shown in Fig. 14, multiple sensing windows show up in the range spectrum plot, from which we can then extract the S11 curve for each sensing layer.

5 Signal Design

5.1 Signal Modeling

FMCW mmWave radar with co-located transmitting and receiving antennas can enable a wide range of smart agricultural sensing applications [21, 47, 52]. It emits periodic chirps that sweep across the mmWave band $x(t)$ and detects the reflected signal $y(t)$:

$$x(t) = A_0 e^{j(\omega(t)*t+\theta_0)}, \quad \omega(t) = \omega_0 + \frac{B}{t_c}t$$
$$y(t) = \sum_{n}^{N} a_n x(t-\tau) \tag{7}$$

where $A(0)$ and a_n are the transmitted power and received power for nth reflection layer, respectively. In our application, this is assumed to be from the range bin of the Director down to the last layer of the sensor. j is the imaginary unit, $theta_0$ is the signal's initial phase, B is the bandwidth, and τ is the time delay from each layer.

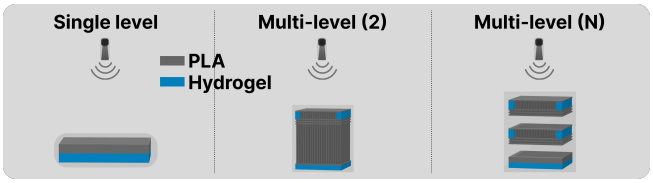

Figure 13: MetaSoil multi-layer sensing hydrogel placement. A single sensor can have two sensing layers that are 10cm apart, while N-layer sensing can be achieved with many sensing layered stacked.

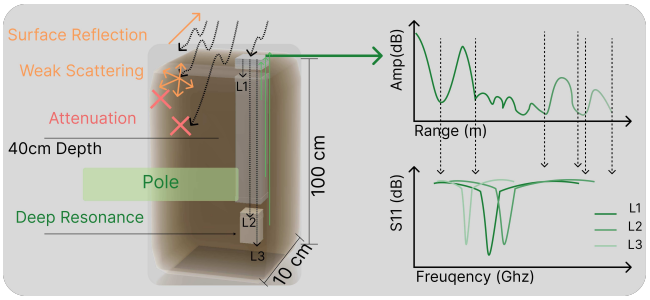

Figure 14: MetaSoil system optimization to multi-layer sensing. Surface reflection and weak scattering can only sense up to <40 cm depth due to soil attenuating RF signal. MetaSoil pole allows multiple layers of soil moisture level to be sensed simultaneously and continuously.

Its maximum range can be calculated as the following [29]:

$$d_{\max} = \left(\frac{\sigma P_t G_{\mathrm{TX}} G_{\mathrm{RX}} \omega^2 T_{\mathrm{meas}}}{(4\pi)^3 \mathrm{SNR}_{\min} kTF}\right)^{\frac{1}{4}} \tag{8}$$

where σ is the radar cross section of the target object, P_t is transmitted power, G_{TX} and G_{RX} are transmitting antenna and receiving antenna gain, respectively. T_{meas} is the measurement time, SNR_{min} is the minimum signal-to-noise ratio, k is Boltzmann's constant, F is noise figure, and T is antenna temperature.

Its range resolution ΔR is directly proportional to its bandwidth and angular resolution. ΔS is defined as the following:

$$\Delta R = \frac{c_0}{2B}, \quad \Delta S = 2Dsin\frac{\theta}{2} \tag{9}$$

where c_0 is the speed of light in free space, B is the bandwidth of the radar TX sweep, D is distance from radar to object, and θ is the antenna beam-width. From which the range of detected object is inferred as:

$$R = \frac{c_0|\Delta t|}{2} = \frac{c_0|\Delta f|}{2(\frac{d(f)}{d(t)})} \tag{10}$$

where Δt is the delay time, Δf is the measured frequency difference, R is the absolute distance of object from radar, and $\frac{df}{dt}$ is the frequency shift per unit time.

5.2 Soil Signature Extraction

Once the FMCW mmWave radar receives the combined response, which occur in units of nanoseconds, we dissect the signal for each layer of soil, and extract soil signature within each layer. From Eq. 7, we can obtain a single n-th layer response y_n assuming line of sight from the radar to the Director:

$$y_n = a_n x(t-\tau) \tag{11}$$

the signal is then normalized to a min-max scale where minimum is free-space, and maximum is from a strong reflector. Similar to Fig. 4(a), in soil sensing application, we use air reflection to model free-space, and use a thin metal sheet to model strong reflector. The remaining time domain signal with embedded soil signature can be transformed into frequency domain with Inverse Fourier Transform (IFFT):

$$Y(\omega) = a_y(\omega)e^{j\omega} \tag{12}$$

where $Y(\omega)$ is the extract return signal at the range, $a_y(\omega)$ is the frequency dependent amplitude response from the soil.

However, this does not translate directly to the $S_11(\omega)$ resonance reading that describes the resonance of the soil layer. To extract the soil resonance, we remove the environment factors by performing a min-max normalization that removes the radar's self interference, as well as background noise[28]:

$$\hat{Y(\omega)} = \frac{Y(\omega) - Y_{min}(\omega)}{Y_{max}(\omega)} \simeq S_{11}(\omega) \tag{13}$$

where $\hat{Y(\omega)}$ is the practical approximation to $S_11(\omega)$ resonance reading. The resulting $\hat{Y(\omega)}$ resonance curve with soil moisture level embedded is a one dimensional array with the size equal to half of radar's number of ADC samples per chirp.

5.3 Regression Model

To extract the exact soil moisture level from the S11 resonance curve, we employ a simple tree structured regression model that learns from prior resonance to moisture level mapping. The model is implemented using scikit-learn RandomForestRegressor library [37]. The model takes the S11 resonance curve $Y(\omega)$ as input and outputs soil moisture level W as follows:

$$\mathrm{W} = \sum_{\omega_0}^{\Omega} c_i \mathbb{I}\{Y(\omega) \in R_i\} \tag{14}$$

where ω_0 is the starting frequency, and the Ω is the last frequency of the S11 resonance curve. $\mathbb{I}\{Y(\omega) \in R_i\}$ is an indicator function that is 1 if $Y(\omega)$ falls into region R_i, and 0 otherwise. c_i are the regression model parameters to solve. The model's training loss is defined through a mean square error function as follows:

$$L_{MSE} = \frac{1}{s}\sum_{i=1}^{S}(y_i - \hat{y}_i)^2 \tag{15}$$

where y_i is the ground truth moisture level, and $\hat{y}_i$ is the regressed moisture level from S11 input.

To this end, we have an end-to-end mmWave sensing system on multi-layers of soil moisture level, with aid from the passive 3D printable metamaterial pole.

6 Evaluation Setup

6.1 Radar setup

We adopt a COTS FMCW radar [8] with a small form factor, which can potentially be carried by mobile autonomous devices (e.g., autonomous drones, robots). The radar has 1 TX and 3 RX antennas arranged in L shape, sweeping the 58-63.5 GHz mmWave band, corresponding a range resolution of 2.7cm. We mount the radar at a default distance of 50 cm above the Director top with 0° incidental angle unless otherwise noted. The director top to sensor bottom distance is 50 cm, unless otherwise noted.

6.2 Metamaterial Pole fabrication

We fabricate MetaSoil's Director, Tunnel and Sensor components using PLA material [4] with a COTS 3D printer[13]. It is worth to note that all components are fully passive, and do not require any power supply. As shown in Fig. 9(a), the Director and Sensor are fixed designs, but the Tunnel is modular, such that the overall length can be adjusted by adding or removing Tunnel pieces. We perform tests on a 10cm×10cm surface area Director/Sensor, with the Director being 2.6cm tall, and the Sensor being 11.4cm tall. Concatenating 5×20cm Tunnel structure, the overall pole is 114cm. The Director and Sensor contain metaatoms that are optimized for 0 to 45 degrees of incident wave at 5 degree intervals. In more detail, each metaatom in the Director contains 6 spacer layers that sandwiches 5 modulating layers. The Sensor contains 5 spacer layers that sandwiches 4 modulating layers. Hydrogel is naturally adhered to the Sensor's first modulating layer (side) as well as the last modulating layer (bottom), allowing multi-layered moisture level sensing 10cm apart.

6.2.1 Hydrogel adaptation. Hydrogel are known for their high water retention capability and durability, and are widely used in agriculture for soil moisture level sensing [16, 26, 32, 53]. We adopt a COTS hydrogel patch [3] in the Sensor to remove soil composition dependency and enhance sensitivity to the moisture level of the metamaterial. As shown in Fig. 15, the transparent hydrogel patch is placed on the Sensor's bottom surface, and the side for multi-layered sensing. Each patch is 1 square inch in size, ≈0.1mm in thickness when completely dry, and ≈3mm in thickness when completely soaked.

6.2.2 Data Collection. We utilize a commercially available wireless soil moisture level sensor [12] based on a capacitive sensor as shown in the top left of Fig. 15 We then use a programmable capacitive sensor with Arduino DC circuit with extensible cables that maps raw capacitive reading onto the COTS moisture level sensor. This enables varied depth ground truth collection. To prevent water from short-circuiting the device while underground, we tape around the exposed circuitry. The programmable capacitive moisture level sensor logs a capacitance that is inversely proportional to the soil moisture level at 1Hz. We perform all data collection and signal processing with a laptop carrying an 8 core mobile CPU and 3.3 GHz clock. Overall, we collected 32 hours of continuous soil moisture level sensing data for general soil moisture level evaluation, and 6 hours for each of subsequent experiments requiring a different setup. We divide all data samples in the same pool into train/valid/test sets with a 60/20/20 split. The data is then fed into a RandomForestRegressor [37] to train and perform a soil moisture reading regression ranging from 0-1. The model predicts soil moisture level based on some deciding factors such as the amplitude of the given curve at specific frequencies. We set the number of estimators to 7, filling up a 3 layer deep tree structure, which directly translates into at most 3 frequencies of interest. This minimizes the computation requirement and the risk of overfitting.

6.2.3 Soil Burying and Irrigation Process. The complete setup is shown in Fig. 15. Multiple 20 cm long poles with fitter design on

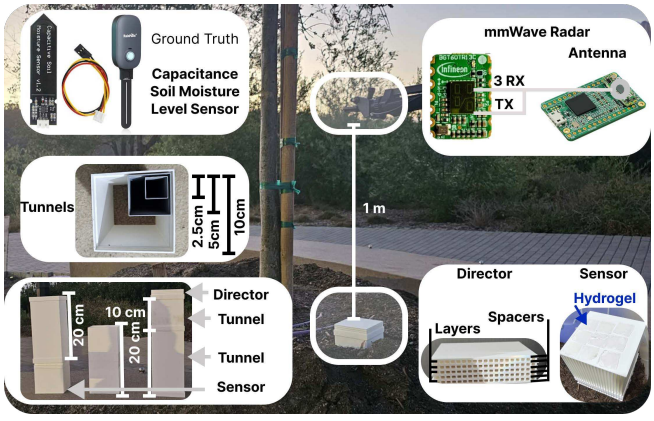

Figure 15: MetaSoil Evaluation setup on natural soil. The length of the pole assembly (consisting Director-Tunnel-Sensor components) can be adjusted by adding or removing one or more of the Tunnel segments.

two ends can be assembled together to form different length poles. The ground truth device is connected with same length cables that extends to sensing depth. The ground truth capacitance reader is placed 5 cm away from the metamaterial pole in the horizontal plane to mitigate the interference of the test device. To manipulate different moisture levels at depth, we manually add 2 Liters of water in between ground truth device and the metamaterial pole and have it sink down. To investigate whether the system can work with different soil, we test it on 3 types of soil (i.e., natural, garden, moss). As shown in Fig. 6, sample 1 is natural soil where it contains large air holes and large particles of irregular shape. Sample 2 is all-purpose garden soil, where it has fewer large particles. Sample 3 is the soil of the peat moss pot that has fine granular soil particles.

6.3 Metrics

To evaluate the sensing performance of a typical soil moisture level sensing system, we adopt the classical measurement metric with accuracy and precision tolerance on top of volumetric water content level. Our ground truth device is a COTS soil moisture level sensor based on a capacitive sensor, which detects volumetric water content level. It has a precision tolerance of ±10% [12]. Hence we adopt the same precision tolerance.

$$\text{Accuracy} = \frac{count(|y - \hat{y}| < P)}{N} \tag{16}$$

where y and $\hat{y}$ represent ground truth and predicted soil moisture level, respectively. P is the precision tolerance, N is the total amount of samples in an experiment.

In addition, to measure the general prediction trend from the S11 curve to the soil moisture level, we also adopt the correlation coefficient (R^2) for the whole data set. The metrics are defined as follows:

$$R^2 = 1 - \frac{\sum_{i=1}^{n}(y_i - \hat{y}_i)^2}{\sum_{i=1}^{n}(y_i - \overline{y})^2} \tag{17}$$

where $\overline{y}^2$ is the average of the ground truth dataset. Higher R^2 value indicates a better overall prediction trend.

7 Evaluation

7.1 General Evaluation

Following the setup in Sec. 6, we evaluate MetaSoil's end-to-end system performance in extrapolating the soil moisture level from the radar signal.

7.1.1 Single vs Double Layer. We first assess the sensor's ability to sense soil moisture level in single layer at a depth of 50 cm. First, we show the correlation between the extracted S11 curve and soil moisture level reading in general trend (Fig. 16(a)) and samples (Fig. 16(b)). Then, we show that over 32 hours of recording, our soil moisture level reading against ground truth device achieves 98.9% accuracy for single layer accuracy at 10 % precision, and 98.8% for double layer accuracy at same precision. The accuracy vs. precision plot is shown in Fig. 17(a) and Fig. 17(b) for single, and double layer performance, respectively.

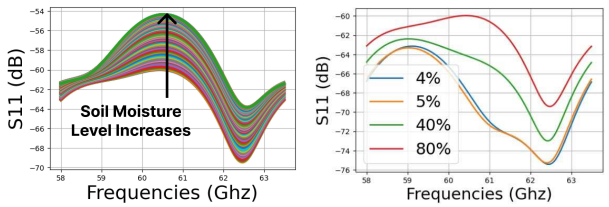

(a) S11 curve as moisture level increases. (b) Samples from resonant curve relative to moisture level.

Figure 16: S11 curves show regions strong correlation to soil moisture level. Samples from resonant curve also shows strong correlation across the whole S11 resonant spectrum.

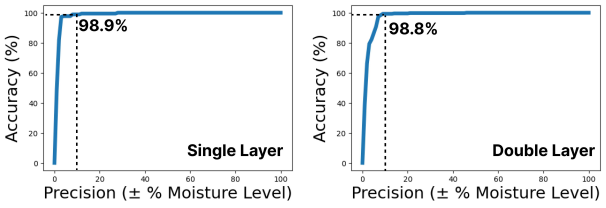

(a) Single layer. (b) Double layer.

Figure 17: Both single level and double level moisture level sensing with MetaSoil Sensor achieves higher then 98% accuracy at ±10% precision.

7.2 Dynamic Range

In real world, different soil depth experiences different ranges of soil moisture. For example, the soil on the surface tends to receive an overflowing amount of irrigation and dry up faster due to direct sun contact ($0 - 100\%range$), the soil directly below the surface

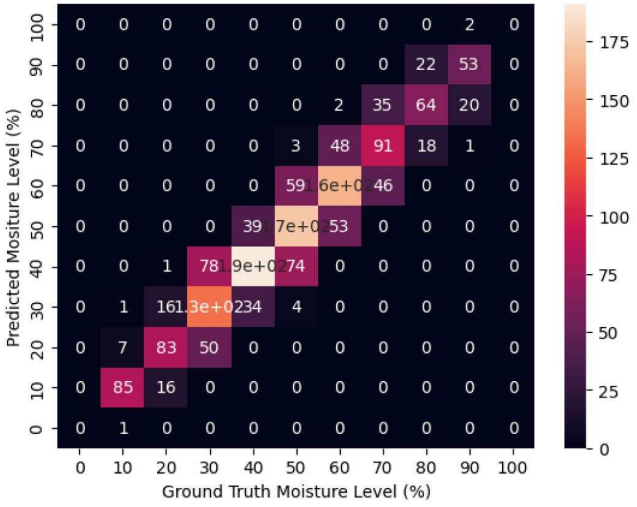

Figure 18: MetaSoil can accurately sense soil moisture level with dynamic range across 5% to 95%.

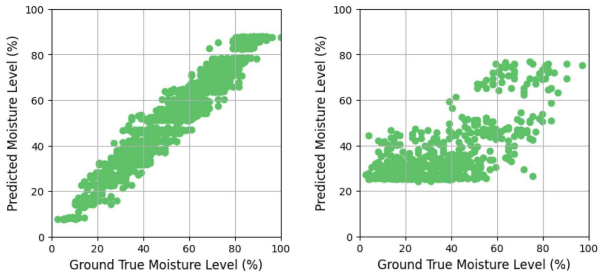

(a) With resonance, $R^2 = 0.98$. (b) Without resonance, $R^2 = 0.6$.

Figure 19: In comparison, MetaSoil achieve superior soil moisture level prediction performance with Director and Sensor co-design, whereas Sensor along under Tunnel suffers from low signal to noise ratio.

level tends to retain some moisture, most of the water runs through (40 – 80%), and the deeper soil tends to stay longer on the heavily moist side (50 – 100%). Thus, it is important to test whether the MetaSoil system is capable of sensing moisture levels in all ranges. To fit the sensing performance into commercially available devices' metrics, Fig. 18 shows a soil moisture level confusion matrix per 10% interval on the sensing accuracy. The range does not cover two ends of the moisture level spectrum due to the difficulty to completely dry soil or soak soil in natural scenario for a long period of time. More specifically, Fig. 19(a) shows that the predicted soil moisture sensor is mostly within the precision tolerance range. This shows that MetaSoil is suitable for working in any moisture level range continuously for smart agriculture applications. It is worthy to mention that the ground truth device has ±10% precision, but it still gives ±1% readings, which lead to the wide standard deviation within ±10% precision. With a more accurate ground truth device, this can be fine tuned. However, we find that trade-off is unnecessary because crops usually have an optimal soil moisture range of 20% [6].

7.3 Effectiveness of the Director

To verify that the Director design is working effectively, we replaced it with a single 2mm thin PLA spacer and ran the simulation in HFSS. As shown in Fig. 20, the RF signal entering from the top

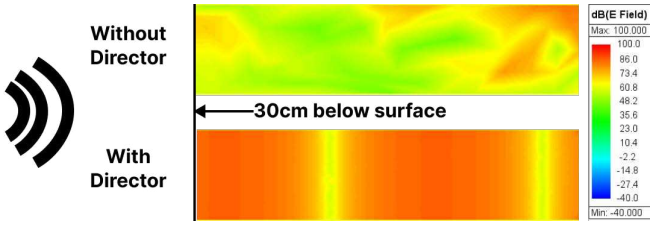

Figure 20: Without Director, we use a 2mm spacer layer to cover the top of the metamaterial pole and simulate the signal propagation, the signal quickly becomes very lossy at 30cm below surface.

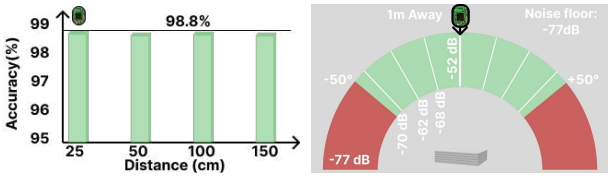

(a) Distance upto 150 cm in air. (b) Angle from ±50° in air.

Figure 21: MetaSoil can robustly identify soil moisture level at various radar distance and angle above the ground.

of the metamaterial pole (i.e., left side in the figure), propagating through the Tunnel, loses 20-30dB over 30 cm distance compared to with Director design. This indicates that our Director is a crucial part of the design, working together with the Tunnel, is effectively propagating the wave to the Sensor and soil layer underneath.

8 Robustness Evaluation

8.1 Impact of Radar Distance/Angle

With radar potentially mounted on mobile devices such as robots, autonomous drones and agricultural vehicles, it is important to evaluate the sensing performance of MetaSoil metamaterial sensor when queried from different distance and angles. As shown in Fig. 21(a), MetaSoil achieves above 98% accuracy with ±10% precision up to 150 cm radar to Director top distance. It's R^2 score is maintained above 0.98 through all distance evaluations. In addition, the Director's implementation on incident angle optimized atoms make its signal reflection signal strength significantly higher than the noise floor even at ±50°, as shown in Fig. 21(b). The Director's design is also symmetric in both azimuth and elevation angles.

8.2 Impact of Sensor Depth

One of the major challenges in soil moisture level sensing is the difficulty to obtain readings from deep soil. MetaSoil explores soil moisture level with a sensor buried at depths ranging from 40 to 120 cm, with a 20 cm interval. For each of the experiments, MetaSoil achieves > 98% accuracy with correlation coefficient R^2 value higher than 0.99, as shown in Fig. 22(b). Given the modular Tunnel and customizable Director/Sensor design, one can quickly prototype a sensor that matches impedance from air above soil

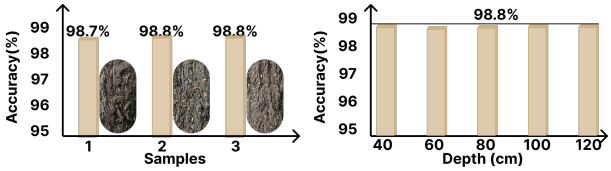

(a) Soil composition. (b) Sensor depth.

Figure 22: MetaSoil can robustly identify soil moisture level with various soil composition and at different Sensor depth. With additional Tunnel segments, MetaSoil's under-surface sensing distance approximates to the radar's maximum operating distance.

surface, to soil layer meters underneath. Overall, MetaSoil proves that it gives reading at different depths with high accuracy.

8.3 Impact of Soil Composition

With hydrogel implementation, MetaSoil aims to eliminate the tedious sensor moisture level calibration process when tested under different soil compositions. MetaSoil is tested with three types of soil with varied particle granularity and water retention capacities. As shown in Fig. 22(a), MetaSoil achieves an accuracy above 98% in sensing soil moisture level on top of each soil sample and has a R^2 score of >0.99. This proves the robustness of MetaSoil on different types of soil, which implies calibration-free deployment on various crop specific soil.

8.4 Impact of Radar Parameters

We further test the robustness of the system with varying radar sensing parameters. The results are shown in Table 1. S11 sample points are directly half of the radar's ADC sampling points due to FFT's symmetric result without padding. In our evaluation, reducing the S11 sampling points to 4 does not reduce the performance of the system. As shown in Fig. 16(a), the trend for resonance amplitude on the S11 scale is consistent throughout the band. The chirp-per-frame parameter reflects the duty cycle that the radar performs while querying the metamaterial pole. With higher chirp rate, noise gets suppressed and signal stands out. However, applying a lower chirp rate to only one chirp per frame does not significantly reduce the sensing accuracy of our system.

9 Discussion and Limitations

9.1 Hydrogel Durability & Chemical Reactivity

Hydrogel is capable of containing water that is 100x its original weight [26], its bio-based polymer composition is proven non-harm [7] when blended with soil to amend the water retention capacity of existing soil. Its low cost, soft, and durable, which can last at least months in large-scale farms [26]. In addition, the hydrogel can serve as a pest bait delivery medium that maintains crop health [54]. Overall, hydrogel-based soil sensing shows a promising direction.

9.2 Tunnel Signal Modeling

mmWave signal can be manipulated with 3D printed patterns inside the tunnel [45]. For specific depth sensing, the walls inside the tunnel can be manufactured with an additional design to improve the signal strength and further enhance the robustness of the system. This will benefit more in multi-layered sensing design where separation of propagation path for different depths can lead to significant SNR increase.

S11 Sample points	Chirps/Frame	Accuracy
512	64	98.8 %
4	64	98.8 %
512	16	98.8 %
512	4	96.1 %
512	1	96.1 %

Table 1: Radar parameter and their corresponding accuracy at ±10% precision. Number of S11 sampling points does not impact performance, whereas reducing the chirps/frame parameter reduces chirp SNR.

9.3 Modular Multi-layer Setup

MetaSoil's signal path along the tunnel is uniformly designed to maximize the SNR of the sensing layers. Given enough signal strength and SNR, a modular design along with tunnel signal modeling can lead to a simpler deployment. However, current setup requires a new prototype for each sensing depth, and with further optimization on the Sensor and Director modeling, it has the potential to reach a uniform design for all depths.

9.4 Expanding to Soil pH and Nutrient

Advancement in material science have led to various sensing capabilities of hydrogels in circuit design [49]. Such capabilities include pH, macronutrient, micronutrient, and other physical properties. However, as shown in Fig. 16(b), the trend of the S11 curve shows a very significant response change due to the change in soil moisture level, the change in NPK level at the ppm level can lead to small amounts of variation, but not as significant as the overall attenuation of the signal due to the presence of water. Temperature caused sensor reading drift can be corrected with the addition of a temperature sensor, which is commonly done in commercial devices, but it is not a contribution in this work.

9.5 Cost analysis

The material cost for printing MetaSoil Tunnel with PLA is $4 for every 20cm of depth,and $2 for a 10cm x 10cm Sensor/Director. The material cost can be further reduced with mass deployments. PLA material is suitable for rapid prototyping, whereas Acrylonitrile Butadiene Styrene (ABS) and carbon fiber enhanced nylon, can achieve greater temperature and corrosion durability with relatively higher cost. Overall, the cost of a single node made from thermoplastic is approximately $10 USD for 1-meter deep sensing per location. This includes the structural costs of the Director, Tunnel, and Sensor, based on 3D printing materials. Due to the Tunnel's modular design, the cost increase for additional depth remains economical. The design can be reused at any site. Compared to other research prototypes and commercial devices with similar sensing capabilities, MetaSoil offers a low-cost solution, primarily due to its minimal manufacturing overhead. This makes it ideal for large-scale deployment in smart agriculture applications.

10 Related Works

10.1 mmWave Metamaterial/Metasurface

mmWave metamaterials have been almost exclusively researched in wireless communication domain for waveform manipulation [27, 35]. Active 2D metamaterial (i.e., metasurface) replacing building walls can perform beam steering for optimizing indoor communication at hardware level[17]. Active metasurface with various antenna on-chip designs can also serve as a waveguide in a wide range of outdoor applications [11]. These systems focus on far-field

System	Sensing Modality	Reader	Passive Sensor	Depth	Multi-L	Capability	CF
Demeter[48]	LoRa TX+Probe	meters	X	$35cm$	X	M	X
[15]	LoRa TX+Probe	meters	X	$30cm$	X	M	X
SoilCares [57]	LoRa TX+IR	meters	X	$20cm$	X	M+NPK	X
[19]	Wi-Fi+Probe	Wired	X	$15cm$	X	M+S	X
CoMEt [34]	GHz RF Radar	On surface	$Tagless$	$38cm$	✓	M	X
[36]	mmWave Radar	On surface	$Tagless$	$Surface$	X	M	X
SoilId [20]	IR-UWB Radar	meters	✓	$30cm$	✓	M	X
LTE-Soil-Meter [25]	LTE+Probe	Wired	X	$15cm$	X	M	X
GreenTag [56]	RFID+Tag	meters	✓	$Surface$	X	M	X
SoilTAG [31]	Wi-Fi+Tag	meters	✓	$75cm$	X	M	X
MetaSoil	**mmWave+Metamaterial**	meters	✓	$\geq$ **1 m**	✓	**M**	✓

Table 2: MetaSoil utilizes passive mmWave sensitive metamaterial sensor that enables over 1m depth of soil moisture level sensing with multi-layer sensing capability, while the mmWave probe can be meters away. Abbr: IR-infrared sensors, Multi-L: Multiple layers sensed simultaneously, Capability(M: Moisture level sensing, NPK: Nitrogen, Phosphorus, Potassium level sensing, S: Salinity). CF: calibration free.

wavefront manipulation, with the goal of focusing on communication tasks. In the near field, [18] proved that the passive mmWave metasurface can help steer the beam for imaging on mm-scale metal reflectors, but with strict lab setup. More closely related to MetaSoil, [10, 33] shows mmWave dielectric resonators in the mmWave band in various sensing applications. However, all these work rely on some active power source to redirect wave for communication driven tasks. In [45] and [41], passive dielectric metasurface is used to reflect the mmWave signal. To our knowledge, MetaSoil is the first work on a passive mmWave metamaterial sensor focusing on wireless sensing tasks with the Sensor mostly in none-line-of-sight to the radar.

10.2 Wireless Soil Sensing

In the past, several categories of wireless sensing systems have been designed to sense soil moisture level. [36] proposed a mmWave radar-based soil moisture sensing system that is limited to the surface level. [34] proposed a sensor-free configuration that offers an algorithmic approach to multilayered moisture level detection, yet its applicability is limited to the soil surface due to its physical attenuation limitations. Similarly, [56] relies on RFID tags in/on pots that are agile but will suffer the same limitation of attenuation when placed underground. Next, [15, 19, 25, 48, 57] utilized sensors/receivers buried under the soil and measures different ratios of attenuation, such a technique requires digging for both placement and maintenance, and the need for power supplies makes it unpractical on a large scale. In [20], UAV onboard IR-UWB radar is used to sense soil moisture level, with a metal reflector under soil surface to increase signal to noise ratio. Lastly, [31] presents a passive metal circuit design that can be buried under the soil with a Wi-Fi antenna that extends over the surface of the soil. This design relies on a metal plate that is completely in contact with the soil and which can easily be corrupted and contaminated. In general, all of the above sensing mechanisms require a calibration scheme for different soil compositions, which is obfuscating the real-world usage. In addition, most systems fail to support crop diversity such as deep-root crops (e.g., grape, olive, almond, trees), which requires depth to be extended to 15 ft [55]. Comparison across all metrics are shown in Table 2. Although each of the work presents their solution to partially solve the problem, their limitations still hinder wide-scale smart agriculture applications.

11 Conclusion

In this paper, we present a fully passive, remote, and 3D-printable metamaterial sensor that allows soil moisture level sensing at the multiple levels, namely MetaSoil. MetaSoil completely gets rid of complex circuit or energy harvesting design, and opts for a dielectric resonator at mmWave frequency. It uses 3D printable PLA metamaterial sensor to perform impedance matching from air above the soil surface, all the way down to deep soil. We studied different soil resonance behaviors and adopted a hydrogel to serve as a mediator material that absorbs and donates water from and to soil/plant root. In addition to metamaterial sensor hardware design and fabrication, we developed a software framework that provides an accurate soil moisture level reading compared to commercial-off-the-shelf capacitance sensors. Extensive experiments demonstrated the effectiveness of MetaSoil. Furthermore, we discussed future potential exploration goals for MetaSoil that can better assist smart agriculture applications. In conclusion, MetaSoil has the potential to serve future smart agricultural and environmental monitoring application needs with its accessibility, accuracy, and flexibility.

Acknowledgment

We thank the anonymous reviewers and shepherd for their valuable feedback. The work reported in this paper is supported in part by the NSF under Grants CNS-1901048, CNS-1925767, CNS-2128588, CNS-2312715, and CNS-2408393.

References

[1] 2013. Powdered water the cure for drought? (July 2013). https://www.iol.co.za/news/powdered-water-the-cure-for-drought-1549671 Accessed: 2024-06-25.
[2] 2023. Safety Data Sheet: S25502. https://www.fishersci.com/content/dam/fishersci/en_US/documents/programs/education/regulatory-documents/sds/chemicals/chemicals-p/S25502.pdf Accessed: 2024-06-25.
[3] 2024. Hydrogel Skin-On-Skin Squares Blister Relief. https://www.elitegymnastics.co.uk/products/hydrogel-skin-on-skin-squares-blister-relief Accessed: 2024-06-25.

[4] 2024. Inland 1.75mm Natural PLA 3D Printer Filament. https://inlandelectronics.com/product/inland-1-75mm-natural-pla-3d-printer-filament/ Accessed: 2024-06-27.

[5] 2024. Smart Agriculture Market Size, Share, Growth Drivers, Industry Report, 2032. https://www.marketsandmarkets.com/Market-Reports/smart-agriculture-market-239736790.html Accessed: 2024-06-25.

[6] AcuRite. 2024. Soil Moisture Guide for Plants and Vegetables. https://www.acurite.com/blog/soil-moisture-guide-for-plants-and-vegetables.html. Accessed: 2024-09-19.

[7] Toby A. Adjuik, Sue E. Nokes, Michael D. Montross, and Ole Wendroth. 2022. The Impacts of Bio-Based and Synthetic Hydrogels on Soil Hydraulic Properties: A Review. Polymers 14, 21 (Nov. 2022), 4721. https://doi.org/10.3390/polym14214721

[8] Infineon Technologies AG. 2024. BGT60TR13C XENSIV™ 60GHz radar sensor for advanced sensing. https://www.infineon.com/cms/en/product/sensor/radar-sensors/radar-sensors-for-iot/60ghz-radar/bgt60tr13c/. Accessed: 2024-06-24.

[9] Mustafa K Taher Al-Nuaimi, Wei Hong, and Xiqi Gao. 2018. 1D and 2D phase gradient perforated dielectric reflective surfaces at mmWave. International Journal of Microwave and Wireless Technologies 10, 4 (2018), 446–452.

[10] Meshari D Alanazi. 2023. A review of dielectric resonator antenna at mm-wave band. Eng 4, 1 (2023), 843–856.

[11] Mohammad Alibakhshikenari, Esraa Mousa Ali, Mohammad Soruri, Mariana Dalarsson, Mohammad Naser-Moghadasi, Bal S Virdee, Caslav Stefanovic, Anna Pietrenko-Dabrowska, Slawomir Koziel, Stanislaw Szczepanski, et al. 2022. A comprehensive survey on antennas on-chip based on metamaterial, metasurface, and substrate integrated waveguide principles for millimeter-waves and terahertz integrated circuits and systems. IEEE Access 10 (2022), 3668–3692.

[12] Amazon. 2024. Product Page for B0CNVPM3FW. https://www.amazon.com/gp/product/B0CNVPM3FW/. https://www.amazon.com/gp/product/B0CNVPM3FW/ Accessed: 2024-06-30.

[13] Bambu Lab. 2024. Bambu Lab A1 3D Printer. https://bambulab.com/en-us/a1 Accessed: 2024-09-19.

[14] Skyler R Brazel. 2023. The Influence of Overwatering, Underwatering, and Waterlogging on the Growth of Kale (Brassica oleracea var. acephala). Mississippi State University.

[15] Zhaoxin Chang, Fusang Zhang, Jie Xiong, Junqi Ma, Beihong Jin, and Daqing Zhang. 2022. Sensor-free soil moisture sensing using lora signals. Proceedings of the ACM on Interactive, Mobile, Wearable and Ubiquitous Technologies 6, 2 (2022), 1–27.

[16] Matthew Chin and Andre Salles. 2021. Tough, yet tender: Scientists firm up research on durable hydrogels. (March 2021). https://www.anl.gov/article/tough-yet-tender-scientists-firm-up-research-on-durable-hydrogels Accessed: 2024-06-25.

[17] Kun Woo Cho, Mohammad H Mazaheri, Jeremy Gummeson, Omid Abari, and Kyle Jamieson. 2023. {mmWall}: A Steerable, Transflective Metamaterial Surface for {NextG}{mmWave} Networks. In 20th USENIX Symposium on Networked Systems Design and Implementation (NSDI 23). 1647–1665.

[18] Hongjun Chu, Jiaran Qi, Shanshan Xiao, and Jinghui Qiu. 2018. A thin wideband high-spatial-resolution focusing metasurface for near-field passive millimeter-wave imaging. Applied Physics Letters 112, 17 (2018).

[19] Jian Ding and Ranveer Chandra. 2019. Towards low cost soil sensing using Wi-Fi. In The 25th annual international conference on mobile computing and networking. 1–16.

[20] Rong Ding, Haiming Jin, Dong Xiang, Xiaocheng Wang, Yongkui Zhang, Dingman Shen, Lu Su, Wentian Hao, Mingyuan Tao, Xinbing Wang, and Chenghu Zhou. 2023. Soil Moisture Sensing with UAV-Mounted IR-UWB Radar and Deep Learning. Proceedings of the ACM on Interactive, Mobile, Wearable and Ubiquitous Technologies 7, 1 (March 2023), 1–25. https://doi.org/10.1145/3580867

[21] Aline Eid, Xuanke He, Ryan Bahr, Tong-Hong Lin, Yepu Cui, Ajibayo Adeyeye, Bijan Tehrani, and Manos M Tentzeris. 2020. Inkjet-/3D-/4D-printed perpetual electronics and modules: RF and mm-wave devices for 5G+, IoT, smart agriculture, and smart cities applications. IEEE Microwave Magazine 21, 12 (2020), 87–103.

[22] Cornell Cooperative Extension. 2024. Soil Organic Matter Fact Sheet. https://franklin.cce.cornell.edu/resources/soil-organic-matter-fact-sheet Accessed: 2024-06-26.

[23] Muhammad Shoaib Farooq, Shamyla Riaz, Adnan Abid, Tariq Umer, and Yousaf Bin Zikria. 2020. Role of IoT technology in agriculture: A systematic literature review. Electronics 9, 2 (2020), 319.

[24] João M Felício, Carlos A Fernandes, and Jorge R Costa. 2016. Complex permittivity and anisotropy measurement of 3D-printed PLA at microwaves and millimeter-waves. In 2016 22nd International Conference on Applied Electromagnetics and Communications (ICECOM). IEEE, 1–6.

[25] Yuda Feng, Yaxiong Xie, Deepak Ganesan, and Jie Xiong. 2022. LTE-Based Low-Cost and Low-Power Soil Moisture Sensing. In Proceedings of the 20th ACM Conference on Embedded Networked Sensor Systems. 421–434.

[26] J Sanz Gómez. 2015. Characterization and effects of cross-linked potassium polyacrylate as soil amendment. University of Seville, Seville, Spain (2015).

[27] Jingwen He, Tao Dong, Baihong Chi, and Yan Zhang. 2020. Metasurfaces for terahertz wavefront modulation: a review. Journal of Infrared, Millimeter, and Terahertz Waves 41, 6 (2020), 607–631.

[28] Ahmed Metwally Hegazy. 2021. Remote material characterization using mmWave FMCW radar with complex baseband. Master's thesis. University of Waterloo.

[29] Ibrahim A Hemadeh, Katla Satyanarayana, Mohammed El-Hajjar, and Lajos Hanzo. 2017. Millimeter-wave communications: Physical channel models, design considerations, antenna constructions, and link-budget. IEEE Communications Surveys Tutorials 20, 2 (2017), 870–913.

[30] International Telecommunication Union. 2017. Electrical Characteristics of the Surface of the Earth. Technical Report ITU-R P.527-4. International Telecommunication Union. https://www.itu.int/dms_pubrec/itu-r/rec/p/R-REC-P.527-4-201706-I!!PDF-E.pdf Accessed: 2024-06-27.

[31] Wenli Jiao, Ju Wang, Yelu He, Xiangdong Xi, and Fuwei Wang. 2023. SoilTAG: Fine-Grained Soil Moisture Sensing Through Chipless Tags. IEEE Transactions on Mobile Computing (2023).

[32] M Hasnat Kabir, Kumkum Ahmed, and Hidemitsu Furukawa. 2017. A low cost sensor based agriculture monitoring system using polymeric hydrogel. Journal of the Electrochemical Society 164, 5 (2017), B3107.

[33] Shady Keyrouz and Diego Caratelli. 2016. Dielectric resonator antennas: basic concepts, design guidelines, and recent developments at millimeter-wave frequencies. International Journal of Antennas and propagation 2016, 1 (2016), 6075680.

[34] Usman Mahmood Khan and Muhammad Shahzad. 2022. Estimating soil moisture using RF signals. In Proceedings of the 28th Annual International Conference on Mobile Computing And Networking. 242–254.

[35] Sunil Kumar and Harbinder Singh. 2022. A comprehensive review of metamaterials/metasurface-based MIMO antenna array for 5G millimeter-wave applications. Journal of Superconductivity and Novel Magnetism 35, 11 (2022), 3025–3049.

[36] Sourav Kumar Pramanik, Md. Shafkat Hossain, and Shekh M. M. Islam. 2024. Noncontact Soil Moisture Estimation Using Continuous Wave Radar and Deep Learning. IEEE Sensors Journal 24, 17 (Sept. 2024), 28419–28426. https://doi.org/10.1109/JSEN.2024.3430531

[37] Scikit learn developers. 2024. sklearn.ensemble.RandomForestRegressor. https://scikit-learn.org/stable/modules/generated/sklearn.ensemble.RandomForestRegressor.html Accessed: 2024-07-01.

[38] Sumit Maya Moreshwar Meshram, Soham Adla, Ludovic Jourdin, and Saket Pande. 2024. Review of low-cost, off-grid, biodegradable in situ autonomous soil moisture sensing systems: Is there a perfect solution? 225 (Oct. 2024), 109289. https://doi.org/10.1016/j.compag.2024.109289

[39] Thomas Meissner and Frank J Wentz. 2004. The complex dielectric constant of pure and sea water from microwave satellite observations. IEEE Transactions on Geoscience and remote Sensing 42, 9 (2004), 1836–1849.

[40] TG Morton, AJ Gold, and WM Sullivan. 1988. Influence of overwatering and fertilization on nitrogen losses from home lawns. Technical Report. Wiley Online Library.

[41] John Nolan, Kun Qian, and Xinyu Zhang. 2021. RoS: passive smart surface for roadside-to-vehicle communication. In Proceedings of the 2021 ACM SIGCOMM 2021 Conference. 165–178.

[42] Almond Board of California. [n. d.]. ALMOND IRRIGATION IMPROVEMENT CONTINUUM. https://www.almonds.com/sites/default/files/2020-02/Almond-Irrigation-Improvement-Continuum.pdf.

[43] IC Paltineanu and JL Starr. 1997. Real-time soil water dynamics using multisensor capacitance probes: Laboratory calibration. Soil Science Society of America Journal 61, 6 (1997), 1576–1585.

[44] Manmath Parida, Aruni Shajkumar, Smita Mohanty, Manoranjan Biswal, and Sanjay K Nayak. 2023. Poly (lactic acid)(PLA)-based mulch films: evaluation of mechanical, thermal, barrier properties and aerobic biodegradation characteristics in real-time environment. Polymer Bulletin 80, 4 (2023), 3649–3674.

[45] Kun Qian, Lulu Yao, Xinyu Zhang, and Tse Nga Ng. 2022. MilliMirror: 3D printed reflecting surface for millimeter-wave coverage expansion. In Proceedings of the 28th Annual International Conference on Mobile Computing And Networking. 15–28.

[46] Amin Ranjbar and Anthony Grbic. 2019. Broadband, multiband, and multifunctional all-dielectric metasurfaces. Physical Review Applied 11, 5 (2019), 054066.

[47] Sandeep Rao. 2017. Introduction to mmWave sensing: FMCW radars. Texas Instruments (TI) mmWave Training Series (2017), 1–11.

[48] Yidong Ren, Wei Sun, Jialuo Du, Huaili Zeng, Younsuk Dong, Mi Zhang, Shigang Chen, Yunhao Liu, Tianxing Li, and Zhichao Cao. 2024. Demeter: Reliable Cross-soil LPWAN with Low-cost Signal Polarization Alignment. In Proceedings of the 30th Annual International Conference on Mobile Computing and Networking. 230–245.

[49] Andreas Richter, Georgi Paschew, Stephan Klatt, Jens Lienig, Karl-Friedrich Arndt, and Hans-Jurgen P Adler. 2008. Review on hydrogel-based pH sensors and microsensors. Sensors 8, 1 (2008), 561–581.

[50] Panagiotis Sarafis and Androula Galiouna Nassiopoulou. 2014. Dielectric properties of porous silicon for use as a substrate for the on-chip integration of millimeter-wave devices in the frequency range 140 to 210 GHz. Nanoscale

research letters 9 (2014), 1–8.
[51] Soils4Teachers. 2024. Physical Properties of Soil. https://www.soils4teachers.org/physical-properties/ Accessed: 2024-06-26.
[52] AG Stove. 2004. Modern FMCW radar-techniques and applications. In First European Radar Conference, 2004. EURAD. IEEE, 149–152.
[53] Qunwei Tang, Jihuai Wu, and Jianming Lin. 2008. A multifunctional hydrogel with high conductivity, pH-responsive, thermo-responsive and release properties from polyacrylate/polyaniline hybrid. Carbohydrate polymers 73, 2 (2008), 315–321.
[54] Jia-Wei Tay, Dong-Hwan Choe, Ashok Mulchandani, and Michael K Rust. 2020. Hydrogels: from controlled release to a new bait delivery for insect pest management. Journal of Economic Entomology 113, 5 (2020), 2061–2068.
[55] University of California Agriculture and Natural Resources. 2023. Growing Grapes in the California Garden. https://cagardenweb.ucanr.edu/Growing_Grapes_in_the_California_Garden/ Accessed: 2024-06-21.
[56] Ju Wang, Liqiong Chang, Shourya Aggarwal, Omid Abari, and Srinivasan Keshav. 2020. Soil moisture sensing with commodity RFID systems. In Proceedings of the 18th International Conference on Mobile Systems, Applications, and Services. 273–285.
[57] Juexing Wang, Yuda Feng, Gouree Kumbhar, Guangjing Wang, Qiben Yan, Qingxu Jin, Robert C Ferrier, Jie Xiong, and Tianxing Li. 2024. SoilCares: Towards Low-cost Soil Macronutrients and Moisture Monitoring Using RF-VNIR Sensing. In Proceedings of the 22nd Annual International Conference on Mobile Systems, Applications and Services. 196–209.
[58] James R Wang and Thomas J Schmugge. 1980. An empirical model for the complex dielectric permittivity of soils as a function of water content. IEEE Transactions on Geoscience and remote sensing 4 (1980), 288–295.
[59] Limin Yu, Wanlin Gao, Redmond R Shamshiri, Sha Tao, Yanzhao Ren, Yanjun Zhang, and Guilian Su. 2021. Review of research progress on soil moisture sensor technology. (2021).